JOURNAL OF GUIDANCE, CONTROL, AND DYNAMICS
Vol. 23, No. 5, September–October 2000

Benchmark Active Controls Technology Model Aerodynamic Data

Robert C. Scott,* Sherwood T. Hoadley,† Carol D. Wieseman,‡ and Michael H. Durham§
NASA Langley Research Center, Hampton, Virginia 23681

The benchmark active controls technology (BACT) model is a part of the Benchmark Models Program (BMP). The BMP is a NASA Langley Research Center program that includes a series of models that were used to study different aeroelastic phenomena and to validate computational fluid dynamics (CFD) codes. The primary objective of BACT testing was to obtain steady and unsteady loads, accelerations, and aerodynamic pressures due to control surface activity to calibrate unsteady CFD codes and validate active control design tools. Three wind-tunnel tests in the Transonic Dynamics Tunnel have been completed. The first and parts of the second and third tests focused on collecting open-loop data to define the model's aeroservoelastic characteristics, including the flutter boundary across the Mach range; these data are presented. An extensive database of over 3000 data sets was obtained. This database includes steady and unsteady control surface effectiveness data, including pressure distributions, and overall model loads due to deflections of a trailing-edge control surface and upper and lower surface spoilers.

Nomenclature

b = model span, 32 in.
C_L = lift coefficient, lift/qS
C_l = rolling moment coefficient, rolling moment/qSb
C_M = pitching moment coefficient, pitching moment/qSc
C_P = pressure coefficient, $(P - P_\infty)/q$
c = model reference chord, 16 in.
M = Mach number
P = pressure
P_∞ = freestream pressure
q = dynamic pressure, $1/2\rho V^2$
S = reference area, bc
V = velocity
x/c = nondimensional chord location
α = angle of attack
δ = deflection of control surface
ρ = density

Introduction

SOME of the interesting aeroelastic phenomena existing in today's aircraft include the following: the classical transonic flutter bucket, wing/store limited amplitude flutter, shock-induced instabilities, and dynamic vortex–structure interactions. Transonic aeroelastic phenomena are often very difficult to understand and analyze. With the rapid increase in computation speeds, new computational fluid dynamic (CFD) codes have matured sufficiently to analyze some of these unsteady transonic phenomena. As these new CFD codes are applied to more complex configurations, a need exists for more experimental data from well-defined and documented configurations to better test and evaluate the analytical results.

Presented as Paper 97-0829 at the 35th Aerospace Sciences Meeting and Exhibit; Reno, NV, 6–10 January 1997; received 6 April 1999; revision received 1 March 2000; accepted for publication 10 March 2000.

*Aerospace Engineer, Aeroelasticity Branch, Structures and Materials Competency. Senior Member AIAA.
†Senior Aerospace Engineer, Data Acquisition and Information Management Branch, Aerodynamics, Aerothermodynamics and Acoustics Competency, Associate Fellow AIAA.
‡Aerospace Engineer, Aeroelasticity Branch, Structures and Materials Competency. Senior Member AIAA.
§Senior Aerospace Engineer, Subsonic Transportation Office. Senior Member AIAA.

The Structures Division of NASA Langley Research Center (LaRC) initiated the Benchmark Models Program (BMP).[1] The goal of the BMP was to obtain experimental data for validating unsteady CFD codes. This program included a series of five models of varying complexity. All of the models have the same planform, but four different airfoil shapes were used. Figure 1 shows a list of the five models and when they were tested.

Apparatus

Model

The benchmark active controls technology (BACT) model is similar in geometry, airfoil section shape, and instrumentation to the previously tested NACA 0012 model presented in Ref. 1. A photograph of the BACT model is shown in Fig. 2. Figure 2 also includes model dimensions and locations of accelerometers. The active controls model extends the unsteady pressure database and the documented flutter instabilities of the NACA 0012 model. Both rigid models have a rectangular wing with a reference chord of 16 in. and a span of 32 in., thus a semispan aspect ratio of 2 and a reference area of 512 in.^{2}. On the BACT model, a trailing-edge control surface and a pair of independently actuated upper and lower surface spoilers have been added. The span of all three control surfaces is 30% of the model span, centered about the model 60% span station. The trailing-edge control surface width is 25% of the model chord. Both spoiler widths are 15% of the model chord and hinged at the 60% chord station. All three control surfaces are moved with independent miniature hydraulic actuators. The actuators allow static control surface displacements or dynamic control surface oscillations about a mean angle. The trailing-edge control surface deflection is mechanically limited to 15 deg either up or down. Each spoiler may be deployed from a 0-deg, stowed position to any angle up to 45 deg. During testing, a transition strip was installed on the model at approximately the 5% chord station on both the upper and lower surfaces.

The combination of a height restriction of 1 in. due to model cavity thickness, the torque requirements of oscillating instrumented control surfaces at high frequencies and the maximum spoiler displacements of up to 45 deg warranted the development of specially designed actuators for both the trailing-edge control surface and the spoilers. A rotary vane actuator was developed for the trailing-edge control surface. The breadboard version of this actuator is shown in Ref. 2. A miniature tandem set of piston actuators was developed for the spoilers. Reference 3 presents the experimental transfer functions for each of the three actuators, assesses the effects of wear and aerodynamic loading, and develops analytical models for each actuator.

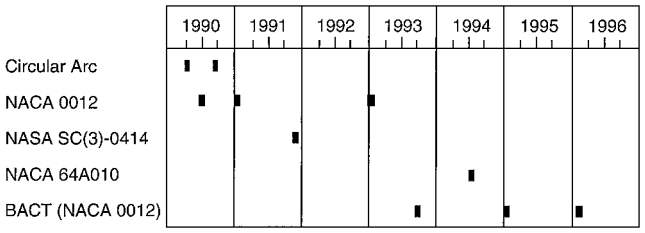

Fig. 1 BMP wind-tunnel tests.

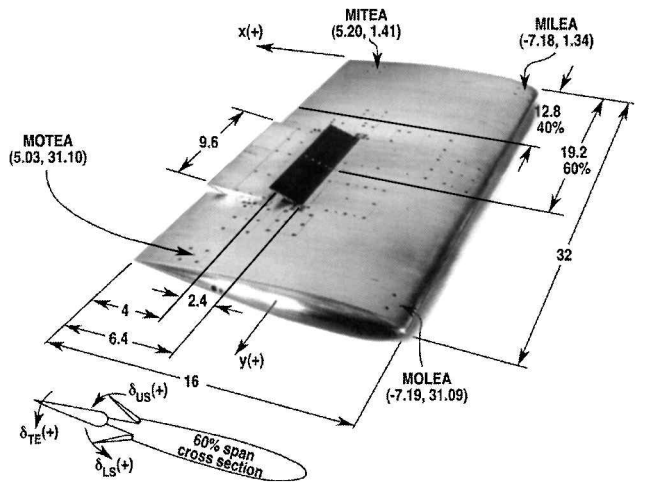

Fig. 2 BACT model showing model inboard leading-edge accelerometer (MILEA), model inboard trailing-edge accelerometer (MITEA), model outboard leading-edge accelerometer (MOLEA), and model outboard trailing-edge accelerometer (MOTEA).

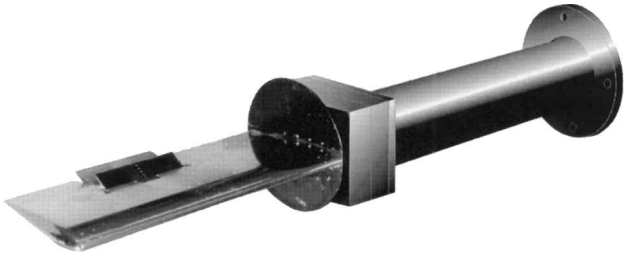

Rigid mount (balance and strut)

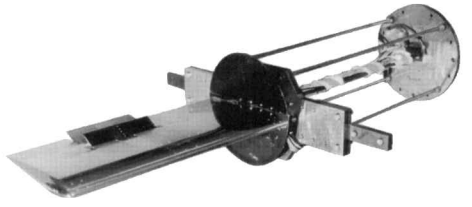

Flexible mount (PAPA)

Fig. 3 BACT model on the rigid and flexible mount systems.

Mount Systems

The mount systems used to support the BACT model consisted of either a rigid or a flexible support and a large splitter plate. Figure 3 shows the BACT model attached to each of the supports, and Fig. 4 shows the model, support, and splitter plate mounted in the wind tunnel. Note that the support is contained in the aerodynamic fairing behind the splitter plate.

The rigid support was only used in the first-half of testing during the 1993 test of the BACT model. It consisted of a rigid strut attached to the tunnel sidewall turntable and a five-degree-of-freedom balance. Five forces were measured with the balance: normal, drag, pitching moment, rolling moment, and yawing moment. For BACT testing, lift was positive up, drag was positive aft, pitching moment was positive leading-edge up, and rolling moment was positive tip up.

Table 1 Measured structural dynamic properties

Property	Plunge mode	Pitch mode
Frequency	3.34 Hz	5.21 Hz
Stiffness	2686 lb/ft	3000 ft-lb/rad
Damping ratio	0.0014	0.0010
Generalize mass	6.08 slug	2.8 slug-ft^2

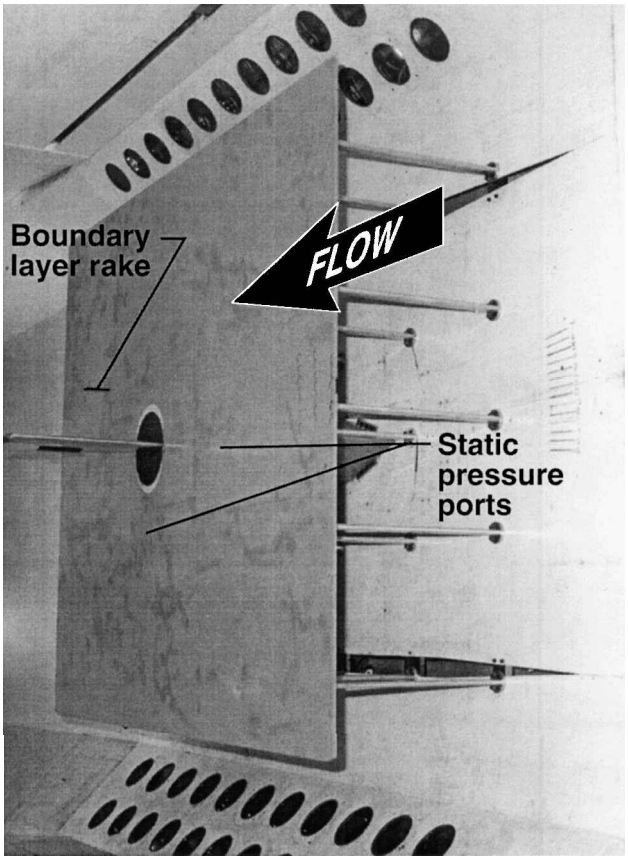

Fig. 4 BACT model installed in TDT.

The flexible support allows for the investigation of aeroelastic instabilities. The pitch and plunge apparatus (PAPA) mount system[4] was developed at LaRC and provides the two flexible degrees of freedom needed for classical flutter. The PAPA consists of a fixed plate attached to the tunnel side-wall turntable, a set of four fixed-end rods, a rectangular shaped drag strut, and a moving plate. The mount system can be dynamically tuned by the addition of masses attached to the moving plate to adjust the model center of gravity and the frequencies of vibration. The center of gravity is located at the model midchord to provide uncoupled wind-off pitch and plunge degrees of freedom. The rigid-body plunge mode consists only of vertical translation of the wing model and the rigid-body pitch mode only of rotation of the wing model about the midchord. The measured structural dynamic parameters are shown in Table 1. The PAPA mount system allows a model angle of attack up to 6 deg, static loads up to 325 lb, and displacements of 1.5 in. either up or down.

Instrumentation

The BACT model instrumentation is designed to obtain unsteady pressure distributions during sustained model oscillations up to and including flutter onset. Differential pressure transducers were installed at two span stations on the model (40 and 60%). These differential transducers were referenced to the tunnel static pressure. The pressure orifice distribution at the 60% span station is similar to the NACA 0012 model. Additional transducers have been included in the area of the three control surface hinge lines. A total of 58 pressure transducers are installed at this span station. An

additional partial chord of 17 transducers were installed inboard of the three control surfaces, at the 40% span station. Figure 5 shows the chordwise locations of the pressure orifices at the 40 and 60% span locations. An additional 20 in situ pressure transducers are mounted in the splitter plate to measure the aerodynamic boundary conditions. A boundary-layer rake with 10 probes is mounted off the splitter plate, aft and slightly above the model, to record the thickness of the wall boundary layer. These can be seen in Fig. 4. Model accelerometers are located near the four corners of the wing to measure the pitch and plunge accelerations and to verify that no local model vibration modes are present in the frequency range of interest, that is, to assure that the model itself remains rigid with only the two degrees of freedom resulting from the PAPA. Potentiometers were used to measure the three control surface deflections. Two pressure transducers per control surface actuator were used to measure the differential hydraulic pressure across the actuator. Table 2 lists the instrumentation used during the tests.

Wind Tunnel

Wind-tunnel testing was conducted in the LaRC Transonic Dynamics Tunnel (TDT).[5] The TDT is a closed-circuit, continuous flow, variable-density, transonic wind tunnel. The slotted test section is 16 × 16 ft square with cropped corners. All slots were open during the BACT wind-tunnel tests. The speed and pressure are independently controllable over a range of Mach numbers from 0.0 to 1.2 (unblocked) and a range of stagnation pressures from near 0 to 1 atm. Either air or a heavy gas can be used as the test medium. For the BACT tests, both air and R-12 were used. The TDT is also equipped with quick-opening bypass valves, which can be activated to reduce rapidly test-section dynamic pressure and Mach number when flutter occurs. The combinations of large-scale, high-speed, heavy gas, variable pressure, and the bypass-valve system make the TDT ideally suited for aeroelastic testing.

Data Acquisition and Reduction

Wing model and mount system sensor time history data (accelerations, loads, and pressures) were acquired at the conditions described in the next section. In all cases, the data were acquired simultaneously, using sample and hold, for all sensor signals at a rate of 500 samples per second on the primary TDT data acquisition system and recorded in digital form on a disk. Records from 10 to 30 s duration were recorded, depending on the test condition. A subset of the acceleration and load signals were also acquired on a secondary system at 200 samples per second, sampled sequentially, but for longer durations.

Table 2 Instrumentation

Transducer	Quantity
Model pressure transducers	75
Splitter plate pressure transducers (1993 test only)	20
Boundary-layer rake pressure transducers (1993 test only)	10
Model accelerometers	4
Control surface accelerometers	6
Control surface potentiometers	3
Control surface command signals	3
Hydraulic pressure transducers	6
Balance components (rigid support only)	5
PAPA strain gauge bridges (flexible support only)	2
PAPA accelerometers (flexible support only)	2
Turntable AOA accelerometer	1
Model AOA accelerometer	1

For all conditions, steady and unsteady, channel statistics (CS), means, minimums, maximums, and standard deviations, were calculated for all analog signals and for pressure coefficients at all locations on the wing. These CS were saved in ASCII files for general use. Tables and plots of the pressure coefficients were also generated and saved for publication and general use using EXCEL® spreadsheet macros and templates. All pressure data were corrected by first applying wind-off, zero dynamic pressure (wind-off-zero) corrections. The balance loads were calculated by removing interactions between the balance signals and recorded for each test condition. Only the uncorrected balance signals, not the corrected balance loads, are available as time histories.

For unsteady data due to an aeroelastic instability, such as flutter, or in response to oscillating control surfaces at a specific frequency, magnitude and phase (MP) with respect to a reference channel at the frequency of interest were also calculated. Once again, tables and plots of MP were also generated and saved for publication and general use.

For unsteady data due to oscillating control surfaces with sweeps or periodic pseudonoise, transfer functions of model response with respect to the control surface motion and actuator transfer functions were calculated using MATLAB®. These transfer functions were plotted and saved on binary files for future reference and documentation. The periodic pseudonoise[6] (PPN) was a specially designed excitation that provided high signal-to-noise ratios with a frequency content specified by the engineer and subject to constraints on control surface rates. It is not truly random. The specific frequency content is based on the frequency resolution, determined by the block size and the Nyquist frequency, and the frequency band of interest.

The raw time history (TH) data are saved in counts along with all engineering unit (EU) conversion information. An interface program, written in C, was developed by NASA to convert the TH data to various ASCII and binary formats, including MATLAB® binary format. A MATLAB-based TDT analysis package was also developed at NASA to convert the data to EUs and perform a multitude of specific analysis options.[7] This TDT analysis package is also able to process and generate the CS and MP data files required by the EXCEL® templates mentioned earlier. Documentation and procedures are available on request to convert the data and perform any of the posttest analysis options discussed herein. Depending on the type of testing, TH, CS, MP, and transfer function (TF) data are available.

Experimental Results

This section of the paper will describe the database of experimental results. The discussion is divided into two parts. The first part describes data obtained on the rigid mount and the second part describes data obtained on the flexible mount. In each case, tables

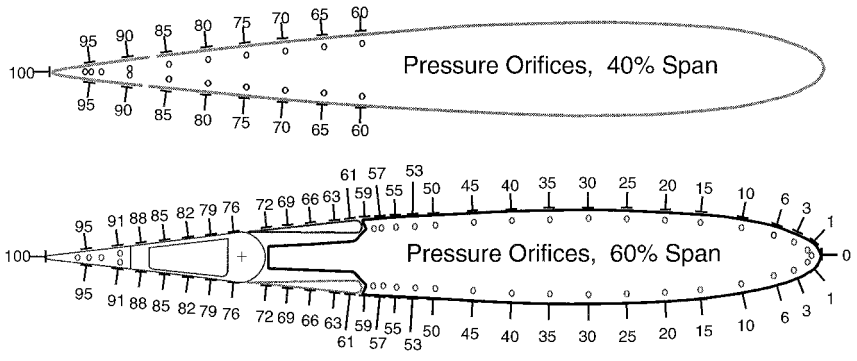

Fig. 5 BACT model orifice locations.

Table 3 Rigid polar data

					Biases		
M	*q*, psf	Type	Polar values	Alpha	TE	US	LS[a]
0.5	93	Alpha	0, 1, 2, 4, 6, 8, 10, 12	——	0	0	0
0.65	145	Alpha	−4, −2, 0, 0.5, 1, 2, 4, 6	——	0, 5	0	0
0.75	156	Alpha	−4, −2, 0, 0.5, 1, 2, 3, 4, 5, 6, 7, 8	——	0	0	0
0.77	141	Alpha	−4, −2, 0, 0.5, 1, 2, 3, 4, 5, 6, 7, 8, 9	——	0	0	0
0.77	143	Alpha	−4, −2, 0, 0.5, 1, 2, 3, 4, 5, 6, 7, 8	——	−5	0, −20, −40	0, 20
0.82	169	Alpha	−4, −2, 0, 0.5, 1, 2, 3, 4, 5, 6, 7, 8, 9, 10	——	0	0	0
0.82	173	Alpha	−4, −2, 0, 0.5, 1, 2, 4	——	5	0	0
0.82	173	Alpha	−4, −2, 0, 0.5, 1, 2, 4	——	0	−20	0
0.82	173	Alpha	−4, −2, 0, 0.5, 1, 2, 4	——	0	0	20
0.9	135	Alpha	0, 0.3, 0.5, 0.8, 1, 1.5, 2, 3	——	0, 2	0	0
0.5	93	TE	−4, −2, 0, 0.5, 1, 2, 4, 6	0	——	0	0
0.65	145	TE	−10, −5, −2, 0, 2, 5, 10	0, 2, 4	——	0	0
0.75	156	TE	−10, −5, −2, 0, 1, 2, 3, 5, 10, 12	0, 2, 4	——	0	0
0.77	145	TE	−10, −5, −2, 0, 0.5, 1, 2, 3, 5, 10, 12	0, 1, 2, 4, 5, 6, 8	——	0	0
0.82	171	TE	−10, −5, −2, 0, 0.5, 1, 2, 3, 5, 10, 12	0, 2, 4	——	0	0
0.9	135	TE	−5, −2, −1, −0.5, 0, 0.5, 1, 1.5, 2, 5	0, 0.5, 1	——	0	0
0.65	145	US	0, −5, −10, −20, −40	0, 4	0	——	0
0.77	150	US	0, −0.5, −1, −2, −5, −10, −15, −20, −25, −35, −43	−2, 0, 2, 4, 5, 6, 8	0	——	0
0.77	150	US	0, −0.5, −1, −2, −5, −10, −15, −20, −25, −35, −43	−2, 0, 2, 4, 5, 6, 8	0	——	0, 5, 10
0.77	150	US	−5, −10, −20	−2, 0, 2, 5	5, 10, 12	——	0
0.82	171	US	0, −1, −2, −5, −10, −15, −20, −43	0, 2, 4	5, 10, 12	——	0, 5
0.9	138	US	0, −1, −2, −3	0, 0.5	0	——	0

[a]Lower spoiler.

Table 4 Unsteady rigid data

					Biases, deg		
M	*q*, psf	Control surface	Excitation description	Alpha, deg	TE	US	LS
0.65	145	TE	Dwell: 2, 5, 10 Hz @ 1, 2, 4 A	0, 4	0	0	0
0.77	140–152	TE	Dwell: 2, 5, 10 Hz @ 1, 2, 4 A	0, 2, 4	0, 5	0, −5, −10, −20	0
0.82	175	TE	Dwell: 2, 5, 10 Hz @ 1, 2, 4 A	0, 4	0	0	0
0.90	138, 175	TE	Dwell: 2, 5, 10 Hz @ 1, 2, 4 A	0, 0.5	0	0	0
0.82	175	TE	LinSS: 0.5–12 Hz @ 1, 2, 4 A	0, 0.5	0	0	0
0.77	144–150	TE	LinSS: 0.5–12 Hz @ 1, 3, 4 A	0	0, 5	0, −5, −10, −20	0
0.77	144–150	TE	LinSS: 0.5–12 Hz @ 1, 3, 4 A	0, 2, 4, 5, 6	0	0, −20	0
0.65	145	TE	LinSS: 0.5–12 Hz @ 4 A	0, 4	0	0	0
0.77	143–150	TE	PPN: 0.5–12 Hz @ 1, 3, 4 A	0	0, 5	0, −5, −10, −20	0
0.77	143–150	TE	PPN: 0.5–12 Hz @ 1, 3, 4 A	2, 4, 5	0	0, −20	0
0.65	145	US	Dwell: 2, 5, 10 Hz @ 1, 2, 4 A	0, 4	0	−10	0
0.77	148–153	US	Dwell: 2, 5, 10 Hz @ 1, 2, 4 A	0, 2, 5	0	−5, −10, −20	0
0.82	175–177	US	Dwell: 2, 5, 10 Hz @ 1, 2, 4 A	0, 4	0	−10, −20	0
0.90	138	US	Dwell: 2, 5, 10 Hz @ 1, 2, 4 A	0, 0.5	0	−2	0
0.65	145	US	LinSS: 0.5–12 Hz @ 2, 10 A	0, 4	0	−10	0
0.77	148–153	US	LinSS: 0.5–12 Hz @ 2, 10 A	0, 2, 5	0	0, −10, −20	0
0.82	175–177	US	LinSS: 0.5–12 Hz @ 2, 10 A	0, 4	0	−10, −20	0
0.90	138	US	LinSS: 0.5–12 Hz @ 2, 10 A	0, 0.5	0	−2	0
0.77	149–178	LS	Dwell: 2, 5, 10 Hz @ 1, 2, 4 A	0, 2, 4, 5	0	0	5, 10, 20

A = Amplitude, Deg.

summarizing the available data sets will be discussed and example plots will be shown. The test medium for all of the following data was a heavy gas, R-12.

Rigid Mount

Data were acquired on the rigid mount for a series of different model angles of attack, with control surfaces having various static displacements, sinusoidal oscillation (dwell), linear sine sweeps (LinSS), and periodic-pseudonoise inputs. The steady and unsteady rigid data sets are summarized in Tables 3 and 4, respectively. The tunnel conditions, model angle of attack, and control surface bias combinations where steady data were acquired are summarized in Table 3. Table 3 is sorted by polar type and Mach number. The polar type identifies the particular parameter that is being varied, such as α, δ_{TE}, δ_{US}, and δ_{LS}. These data can best be viewed by looking at plots of the mean loads and mean pressures. Figure 6 shows the lift, pitching moment, and rolling moment coefficients as functions of angle of attack for the Mach 0.77 alpha polar. As can be seen, all increase with increasing alpha. The drag polar plot, displaying lift vs drag, corresponding to this same tunnel condition for varying

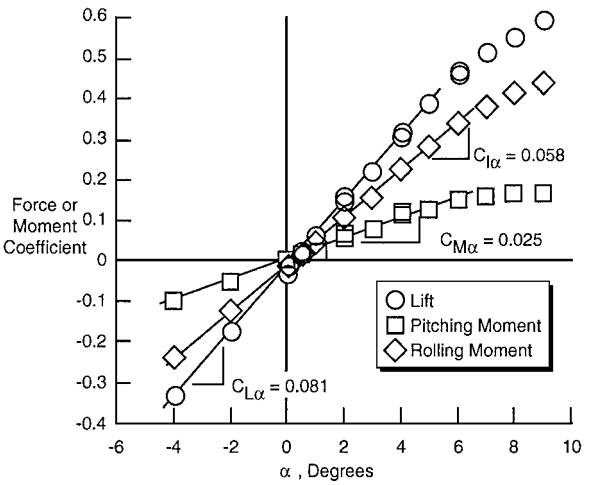

Fig. 6 Force and moment coefficients as a function of alpha, M = 0.77 and q = 141.5 psf.

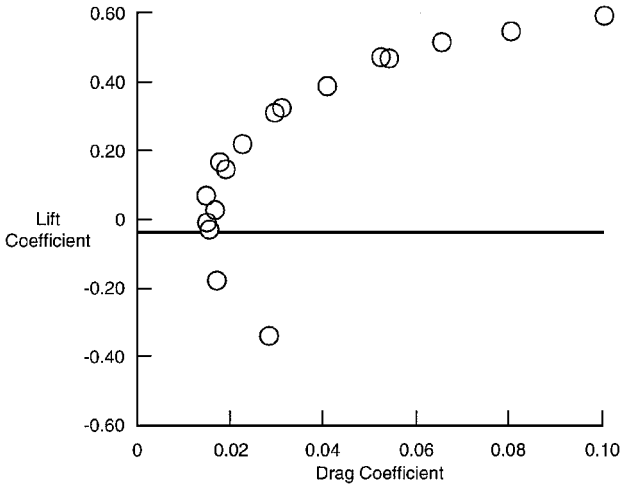

Fig. 7 Drag polar for alpha variation, $M = 0.77$ and $q = 141.5$ psf.

alpha is shown in Fig. 7, and the mean pressures for both the upper and lower model surfaces for alpha varying between −4 and 8 deg is shown in Fig. 8. Two key features of Fig. 8 are that for angles greater than 2 deg in magnitude, a shock develops on one of the wing surfaces and the dip in the pressures near the leading edge is caused by the presence of the transition strip. An upper spoiler polar and a trailing-edge control surface polar are shown in Figs. 9 and 10, respectively. Both Figs. 9 and 10 are for $\alpha = 5$ deg so that the control surface effect on the shock could be demonstrated. The loads due to trailing-edge control surface deflection and upper spoiler deflection are shown in Figs. 11 and 12, respectively. As can be seen, lift and rolling moment increase with increasing deflection. In the case of the upper spoilers, this implies that lift and rolling moment increase as the spoiler goes from fully deployed to stowed. The relationship between load and deflection is fairly linear for the trailing edge control surface and nonlinear for the upper spoiler (US). The pitching moment is not greatly affected by changes in deflection of either control surface.

The unsteady rigid data are summarized in Table 4. These data are organized by control surface used, excitation type, and Mach

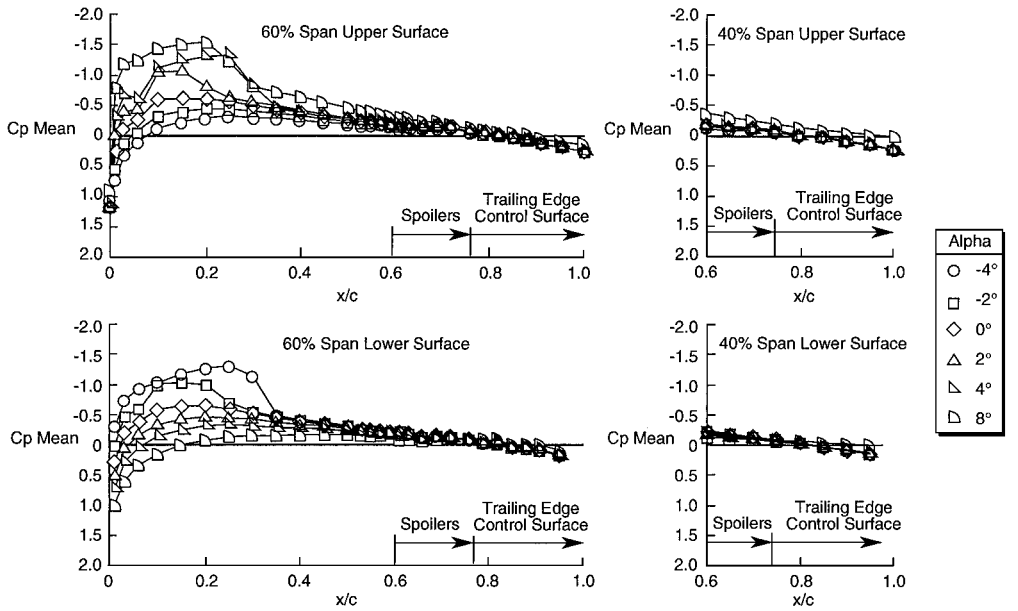

Fig. 8 Variation of upper- and lower-surface mean pressures with alpha, $M = 0.77$ and $q = 141.5$ psf.

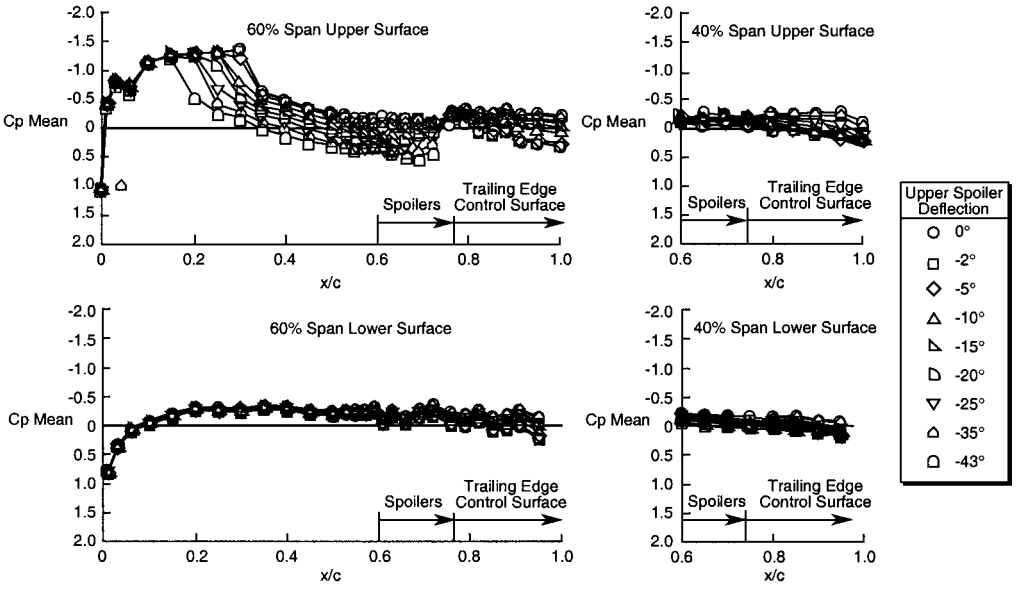

Fig. 9 Variation of upper- and lower-surface mean pressures with US control surface deflection: $\alpha = 5$ deg, $M = 0.77$, and $q = 152.1$ psf.

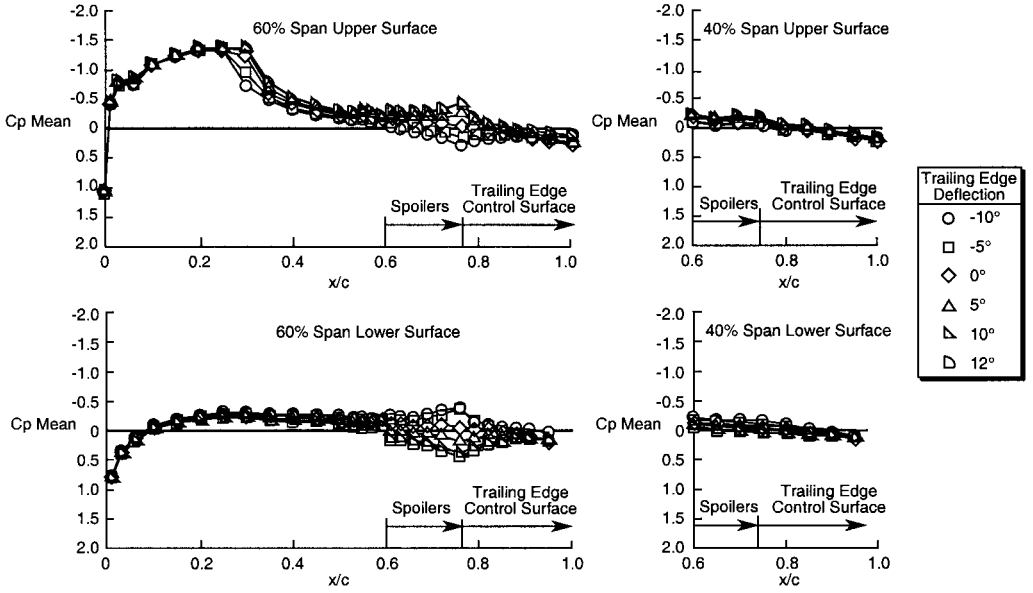

Fig. 10 Variation of upper- and lower-surface mean pressures with TE deflection: α = 5 deg, M = 0.77, and q = 145.7 psf.

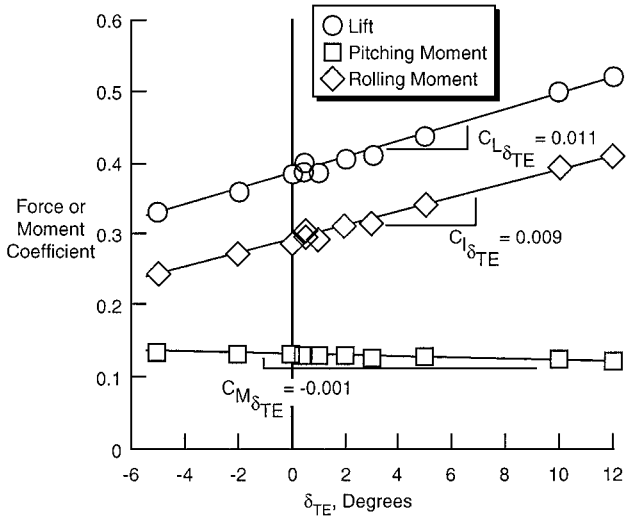

Fig. 11 Force and moment coefficients as a function of TE deflection: α = 5 deg, M = 0.77, and q = 145.7 psf.

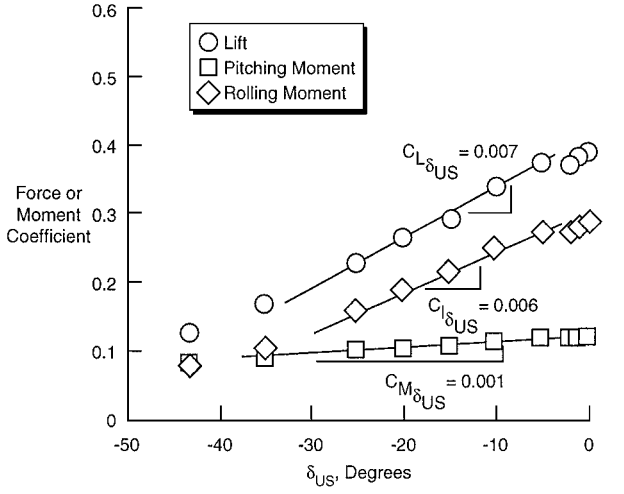

Fig. 12 Force and moment coefficients as a function of US control surface deflection: α = 5 deg, M = 0.77, and q = 152.1 psf.

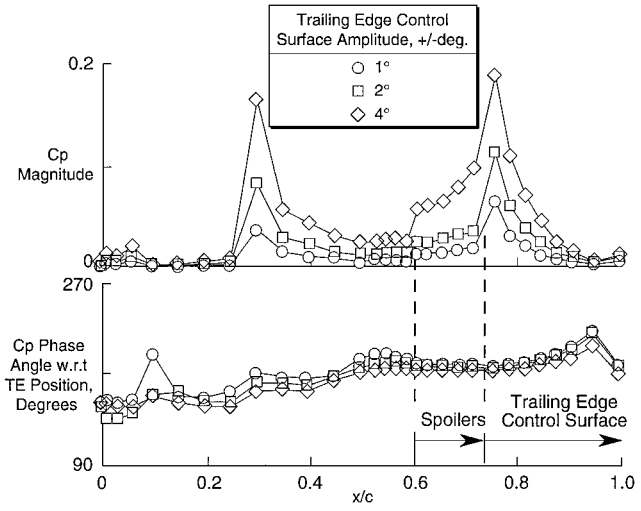

Fig. 13 Unsteady upper-surface pressures at 60% span station due to TE dwell at 5 Hz: α = 5 deg, M = 0.77, and q = 153 psf.

number. Most of these data consist of responses to dwells and LinSS; however, several PPN excitations were also employed for comparison purposes. Because the PPN excitation does not dwell on any one frequency, higher signal-to-noise ratios can be obtained when testing near instabilities, but in general the responses are not as clean and require more averages than linear sine sweeps to clean up the results. The dwell data are most easily examined by viewing the results in the frequency domain at the excitation frequency. Figure 13 shows the magnitude and phase of the pressure coefficients for a 5-Hz oscillation of the trailing-edge control surface. There are two peaks in the magnitude plot. One occurs at approximately the 30% chord station where the motion of the trailing edge control surface is moving the upper surface shock wave back and forth over the pressure transducer. The other peak occurs on the control surface near the hinge line. Although not shown, linear sine sweep and PPN timehistory allow for the calculation of frequency-response functions for any or all of the pressure transducers and loads across a frequency range of interest.

Flexible Mount

Three types of instabilities were encountered with the BACT/PAPA system. One was a classical flutter instability where the two primary vibratory modes coalesce. The other instabilities were a plunge instability and a stall instability. The tunnel conditions where instabilities occurred are shown in Fig. 14. The boundaries where

Table 5 Unsteady PAPA data, zero TE Bias

M	q, psf	Control surface	Excitation description, Hz	Alpha, deg	Biases, deg	
					US	LS
0.5, 0.65, 0.7, 0.75, 0.77, 0.8, 0.94	101–140	TE	Dwell: 3.2–5	0, 2	0	0
0.5, 0.65, 0.70, 0.75, 0.77, 0.8, 0.88	101–130	TE	LinSS: 2–8 and 0.5–12	2	0	0
0.5, 0.65, 0.7, 0.75, 0.77, 0.8, 0.84, 0.88, 0.94	101–135	TE	PPN: 2–8 and 0.5–12	0, 2	0, −5, −40	0, 5, 40
0.65, 0.85	74, 114	TE	LinSS: 0.5–12	1.7	0, −5, −10, −15, −20	0, 5, 10, 15, 20
0.5, 0.65, 0.7, 0.75, 0.77, 0.8, 0.88	116–130	US	Dwell: 2.0–10	2	0, −5, −10	0
0.5, 0.65, 0.70, 0.75, 0.77, 0.80, 0.88	116–130	US	LinSS: 0.5–12	2	0, −3, −5, −10	0
0.5, 0.65, 0.7, 0.75, 0.77, 0.8, 0.88	115–133	US	PPN: 2–8 and 0.5–12	2	0, −3, −5, −10	0
0.65, 0.84	115, 135	US	PPN: 2–8 and 0.5–12	0, 2	0, −10	0, 10
0.65, 0.7, 0.75, 0.77, 0.8, 0.88, 0.92	101–130	US + LS[a]	Dwell: 3–5	0, 2	0, −3, −5, −10	0, 3, 5, 10
0.5, 0.65, 0.70, 0.75, 0.77, 0.80, 0.88	103–130	US + LS	LinSS: 2–8 and 0.5–12	2	0, −3, −5, −10	0, 3, 5, 10
0.5, 0.65, 0.7, 0.75, 0.8, 0.84, 0.88, 0.93	101–130	US + LS	PPN: 2–8 and 0.5–12	0, 2	0, −2, −3, −10, −20, −40	0, 2, 3, 10, 20, 40
0.65, 0.85	74, 114	US + LS	LinSS: 0.5–12	1.7	−10	10
0.92	124	US − LS[b]	Dwell: 3	0	−2	2
0.65	115	US − LS	LinSS: 0.5–12	2	−10	10
0.65	113	LS	Dwell: 3.44 and 4.56	2	−2	2
0.65	113	LS	PPN: 0.5–12	2	0	10

[a]Motion of US and LS is in the same direction. [b]Motion of US and LS is in opposing directions.

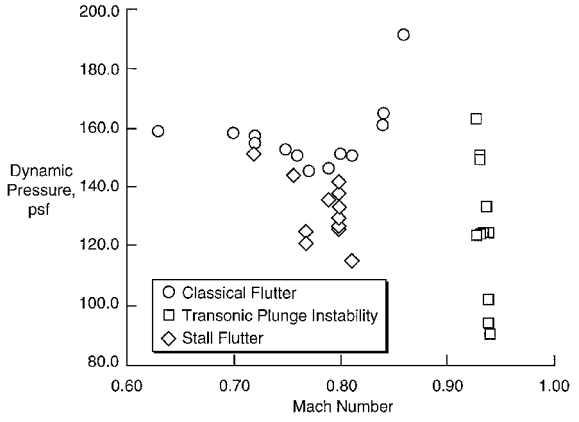

Fig. 14 BACT instabilities.

these instabilities occurred are similar to the ones encountered in the previous NACA 0012 benchmark model test described in Ref. 8. Timehistory data were acquired at these points and at some of these points, magnitude and phase of pressures were also calculated at the frequency of the instability.

The classical flutter boundary for the BACT model is represented by the circles in Fig. 14. The open-loop model is stable below this boundary and unstable above. This boundary was obtained with zero bias on the control surfaces and an angle of attack large enough to create lift approximately equal to weight of the model. There is a transonic dip near $M = 0.77$ followed by a sharp upward turn of the boundary near $M = 0.8$. For the $M = 0.63$ and $q = 158$ psf flutter point, magnitude and phase at the flutter frequency of 4.3 Hz are shown in Fig. 15. The zero magnitude data points in Fig. 15 correspond to transducers that were no longer functioning. Before each wind-tunnel run, 1-psi checks were performed to evaluate the transducers calibration and functionality. This provides with certainty the accuracy of each transducer for steady data; however, a transducer can pass this test and still be inaccurate for unsteady data. An example of this is the transducer on the trailing-edge control surface that does not fit the trend. This transducer probably has a partially blocked reference tube rendering it unreliable for unsteady data.

Occurrences of a plunge instability are indicated by the squares in Fig. 14. This instability occurs in a narrow transonic Mach number range around 0.92 and consists primarily of the plunge mode at a frequency around 3.5 Hz. Because this instability is caused by the fore and aft motion of symmetric shocks on the upper and lower surface of the wing, it is very sensitive to any biases and does not occur with nonzero control surface bias or nonzero alpha.

Occurrences of stall flutter are indicated by the diamonds in Fig. 14. This instability is caused by wing stall occurring during a portion of the pitch oscillation cycle. The primary mode in this instability is the pitch mode at a frequency around 5 Hz. This instability could be encountered at most tunnel conditions where high angles of attack could be attained without exceeding the load limits for the PAPA mount. Generally stall flutter was encountered at mean angles exceeding 4 deg.

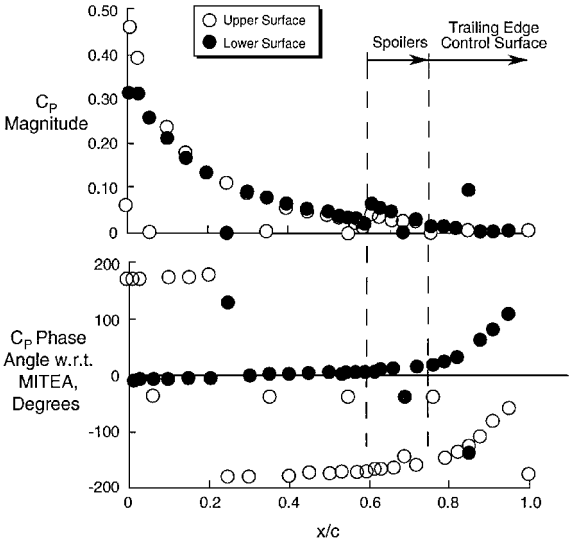

Fig. 15 Unsteady pressures at 60% span acquired during flutter, M = 0.63, and q = 158 psf.

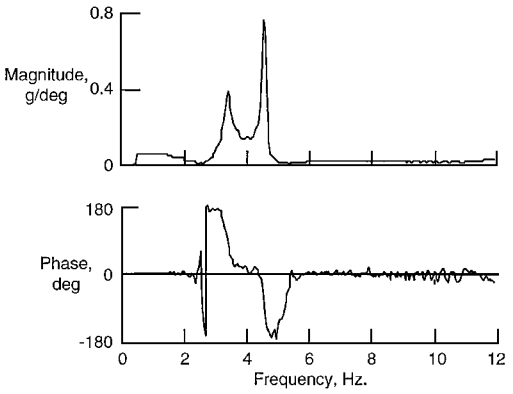

Fig. 16 Acceleration frequency-response function due to US + LS, M = 0.65, and q = 114 psf.

Below the flutter boundary, control surface inputs were used to excite the BACT model so that transfer functions could be calculated and compared with results of aeroservoelasticcodes. The types of excitations along with the corresponding tunnel conditions and biases are summarized in Table 5. An example frequency-response function calculation is shown in Fig. 16. Here, both spoilers were

biased 10 deg into the airstream, and their input was a linear sine sweep. Note that, for this condition, the two primary modes of motion, pitch and plunge, still exist as distinct modes as indicated by the separate peaks in the magnitude plot. Reference 9 made extensive use of these data to compare with aeroservoelastic models of the BACT plant.

Conclusions

The results from three BACT tests are available for use to better understand the classical and nonlinear flutter mechanisms encountered in transonic flows, to evaluate control surface and spoiler effectiveness, to study controllability and linearity issues, and to assess, expand, and validate modeling and design tools for applying active control concepts to alleviate aeroelastic phenomena.

During the three wind-tunnel tests in the TDT, an extensive database of over 3000 data sets was obtained for the BACT model. Transonic, subsonic, attached, and separated flow conditions were explored. This experimental database, which is available to correlate with analytical predictions, provides unique transonic and subsonic measurements for both the validation of CFD codes and control law design. Aerodynamic loads and wing pressures were acquired for various combinations of TE deflection, spoiler deflection, and wing angle of attack. The stability boundaries for classical flutter and for other nonlinear aeroelastic instabilities in transonic flow were also explored and measured. Measurements were acquired to evaluate the dynamic response characteristics due to various combinations of excitation and static deployment of the three control surfaces. An extensive database of transient and frequency-response data were also acquired for subsonic through transonic Mach numbers over a wide range of dynamic pressures. The combination of force testing and pressure measurements will permit detailed diagnostics and the exploration of limitations for computer program applications.

References

[1]Rivera, J. A., Jr., Dansberry, B. E., Farmer, M. G., Eckstrom, C. V., Seidel, D. A., and Bennett, R. M., "Experimental Flutter Results with Steady and Unsteady Pressure Measurements of a Rigid Wing on a Flexible Mount System," AIAA Paper 91-1010, April 1991.

[2]Durham, M. H., Keller, D. F., Bennett, R. M., and Wieseman, C. D., "A Status Report on a Model for Benchmark Active Controls Testing," AIAA Paper 91-1011, April 1991.

[3]Waszak, M. R., "Parameter Estimation and Analysis of Actuators for the BACT Wind-Tunnel Model," AIAA 96-3362, 1996.

[4]Farmer, M. G., "A Two-Degree-of-Freedom Flutter Mount System with Low Damping for Testing Rigid Wings at Different Angles of Attack," NASA TM 83302, 1982.

[5]"The Langley Transonic Dynamics Tunnel," NASA Langley Research Center Working Paper LWP-799, Sept. 1969.

[6]Pototzky, A. S., Wieseman, C. D., Hoadley, S. T., and Mukhopadhyay, V., "On-Line Performance Evaluation of Multi-Loop Digital Control Systems," *Journal of Guidance, Control, and Dynamics*, Vol. 15, No. 4, 1992, pp. 878–884.

[7]Wieseman, C. D., and Hoadley, S. T., "Versatile Software Package for Near Real-Time Analysis of Experimental Data," AIAA Paper 98-2722, June 1998.

[8]Rivera, J. A., Jr., Dansberry, B. E., Bennett, R. M., Durham, M. H., and Silva, W. A., "NACA 0012 Benchmark Model Experimental Flutter Results with Unsteady Pressure Distributions," NASA TM 107581, March 1992.

[9]Waszak, M. R., "Modeling the Benchmark Active Control Technology Wind-Tunnel Model for Application to Flutter Suppression," AIAA Paper 96-3437, July 1996.